Journal of Organometallic Chemistry 716 (2012) 19–25

Contents lists available at SciVerse ScienceDirect

Journal of Organometallic Chemistry

journal homepage: www.elsevier.com/locate/jorganchem

Electrocatalytic and photocatalytic reduction of carbon dioxide to carbon monoxide using the alkynyl-substituted rhenium(I) complex (5,5′-bisphenylethynyl-2,2′-bipyridyl)Re(CO)$_3$Cl

Engelbert Portenkirchner [a,*], Kerstin Oppelt [b], Christoph Ulbricht [a,c], Daniel A.M. Egbe [a], Helmut Neugebauer [a], Günther Knör [b], Niyazi Serdar Sariciftci [a]

[a] Linz Institute for Organic Solar Cells (LIOS), Physical Chemistry, Johannes Kepler University Linz, A-4040 Linz, Austria
[b] Institute of Inorganic Chemistry, Johannes Kepler University Linz, A-4040 Linz, Austria
[c] MEET Battery Research Centre, Institute of Physical Chemistry, University of Muenster, D-48149 Muenster, Germany

ARTICLE INFO

Article history:
Received 10 March 2012
Received in revised form
15 May 2012
Accepted 20 May 2012

Keywords:
CO_2 reduction
Catalysis
Photochemistry
Rhenium complexes
Electrochemistry
FTIR absorption measurements

ABSTRACT

The rhenium complex *fac*-(5,5′-bisphenylethynyl-2,2′-bipyridyl)Re(CO)$_3$Cl was used as a novel catalyst for the electro- and photochemical reduction of CO_2 to CO in homogeneous solution. The results were compared to (2,2′-bipyridyl)Re(CO)$_3$Cl as a benchmark compound. Cyclic voltammetric studies as well as bulk controlled potential electrolysis experiments were performed using a CO_2 saturated solution in acetonitrile. (5,5′-bisphenylethynyl-2,2′-bipyridyl)Re(CO)$_3$Cl showed a 6.5-fold increase in current density under CO_2 at −1750 mV versus normal hydrogen electrode (NHE) as compared to the operation without CO_2. Quantitative analysis by gas chromatography (GC) and infrared spectroscopy showed a Faradaic efficiency of around 45% for the formation of CO.

1. Introduction

The current energy supply of human society is mainly based on fossil fuels like coal, oil and gas which are related to several problems. The reserves are decreasing and their final depletion seems to be just a matter of time [1].

In addition, the combustion of fossil fuels leads to the emission of CO_2, which is considered as a main source for global warming caused by the greenhouse effect [2]. The demand for energy is steadily increasing. Renewable energy appears to be the only sustainable solution. However, since the availability from renewable sources such as wind and solar energy is variable and often does not meet with the time and local needs, efficient energy storage and transport are critical issues [3–5]. Therefore recycling of carbon dioxide by catalytic conversion to gaseous or liquid fuels using renewable energy has received increasing interest in the past years [6].

An efficient way of transforming CO_2 into a synthetic fuel using renewable energy would address both problems simultaneously:

Synthetic fuels can be produced CO_2-neutral and fully sustainable. These fuels can store renewable energy chemically bound, ready to transport and/or use applying existing infrastructures and techniques.

The electrochemical reduction of CO_2 usually requires a high potential of nearly −2 V vs. NHE for a one electron process. By performing a two electron or proton coupled multi-electron CO_2 reduction, however, the required potential can be lowered significantly as can be seen in Table 1 [7].

In reality however, the actual reduction potentials are much higher than the Nernst potential due to barrier induced overpotentials. For lowering the actual redox potential of the CO_2-reduction process, suitable catalysts are required [11–14]. Concerning the generation of CO from carbon dioxide, metal complexes with bipyridine ligands are among the most promising candidates for homogeneous catalysis in terms of activities and lifetimes [15,16]. Up to now, mainly rhenium- and ruthenium-based systems have been reported for their ability to electrochemically or photochemically accelerate the reduction of CO_2 to CO. Carbon monoxide itself can be used as a precursor compound for fuel synthesis processes, where CO and H_2 are mixed as syn-gas to form hydrocarbons such as methane or methanol [17].

* Corresponding author. Tel.: +43 732 24 68 8854; fax: +43 732 24 68 8770.
E-mail address: engelbert.portenkirchner@jku.at (E. Portenkirchner).

0022-328X/$ – see front matter © 2012 Elsevier B.V. All rights reserved.
http://dx.doi.org/10.1016/j.jorganchem.2012.05.021

Table 1
Redox potentials vs. NHE for the one- and multi-electron reduction of CO_2 in an aqueous solution at pH 7 [8,20].

Redox reaction	E^0/V	
$CO_2 + e^- \rightarrow CO_2^-$	−1.90	(1)
$2CO_2 + 2e^- = CO + CO_3^{2-}$	−0.65	(2) [9,10]
$CO_2 + 2H^+ + 2e^- = HCOOH$	−0.61	(3)
$CO_2 + 2H^+ + 2e^- = CO + H_2O$	−0.53	(4)
$CO_2 + 4H^+ + 4e^- = HCHO + H_2O$	−0.48	(5)
$CO_2 + 6H^+ + 6e^- = CH_3OH + H_2O$	−0.38	(6)
$CO_2 + 8H^+ + 8e^- = CH_4 + H_2O$	−0.24	(7)

Schanze et al. studied the excited state properties of several different rhenium bipyridine complexes in great detail [18]. Catalytic effects on the CO_2 reduction have also been extensively investigated and improved in the past [19,20]. The parent complex (2,2′-bipyridyl)Re(CO)$_3$Cl (**1**), which was characterized in this context for the first time by Ziessel and Lehn et al. in 1984 demonstrates high Faradaic efficiencies and no significant decrease in performance due to catalyst degradation over several hours [19,21].

Recently, our group reported the synthesis, structure, photophysics, and spectroscopic characterization of the modified rhenium complex (5,5′-bisphenylethynyl-2,2′-bipyridyl)Re(CO)$_3$Cl (**2**), carrying additional alkynyl substituents at the acceptor ligand [22]. This new compound (Scheme 1) has an extended conjugated π-electron system that increases the optical absorption in the visible spectral range which was assumed be a clear benefit for photocatalytic applications.

In the present work, we report results on compound **2** studied by cyclic voltammetry to determine its catalytic activity for CO_2 reduction to CO according to reaction (2) in Table 1. Samples were taken from the gaseous phase and analysed by GC and Fourier transform infrared (FTIR) measurements. The reduction potential, electronic absorption and Faradaic efficiency were compared with the results obtained for compound **1**.

2. Experimental

2.1. General experimental procedures

Unless otherwise stated, all chemicals and solvents were purchased from commercial suppliers in reagent or technical grade quality and directly used as received: Re(CO)$_5$Cl (Aldrich), 2,2′-bipyridine (Fluka), water free Toluene (Aldrich). ^{1}H and ^{13}C NMR spectra were recorded with a Bruker Avance DPX200 NMR-Spectrometer. Electronic absorption measurements were performed in 1 cm quartz glass cuvettes at 298 K with a Cary 3G UV–visible spectrometer.

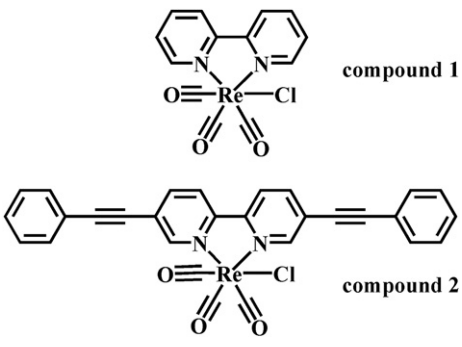

Scheme 1. Chemical structures of (2,2′-bipyridyl)Re(CO)$_3$Cl (**1**) and (5,5′-bisphenylethynyl-2,2′-bipyridyl)Re(CO)$_3$Cl (**2**).

2.2. Syntheses

Manipulations were performed under N_2 flow. The solvents were degassed under heating.

2.2.1. (2,2′-Bipyridyl)Re(CO)$_3$Cl (*1*)

The rhenium complex **1** was prepared with slight modifications to literature methods [23,36]. An equimolar amount of Re(CO)$_5$Cl (0.304 g, 0.84 mmol) and 2,2′-bipyridine (0.131 g, 0.84 mmol) was dissolved in hot toluene (50 ml). The reaction mixture was stirred under reflux for 2 h. Afterwards the solution was removed from the heat source and cooled down by an ice–salt mixture. The product precipitated from solution as a yellow powder and was filtered off. The powder was further dried at a rotary evaporator (5 mbar for 1 h). Pure product was isolated from the reaction with an overall yield of 92%.

^{1}H NMR (200 MHz, CD_3CN): δ/ppm = 7.62 (t, 2H, bipy-H5 and 5′), 8.18 (t, 2H, bipy-H4 and 4′), 8.41 (d, 2H, bipy-H6 and 6′), 9.00 (d, 2H, bipy-H3 and 3′).

2.2.2. (5,5′-Bisphenylethynyl-2,2′-bipyridyl)Re(CO)$_3$Cl (*2*)

The synthesis and characterisation of the rhenium complex **2** were published by K. Oppelt et al. in 2011 [22] The data for ^{1}H NMR and ^{13}C NMR are as follows:

^{1}H NMR (200 MHz, CD_3CN): δ/ppm = 7.45 (m, 6H, phen-H3 and 3′, 4 and 4′, 5 and 5′), 7.65 (m, 4H, phen-H2 and 2′, 6 and 6′), 8.35 (dd, 2H, bipy-H4 and 4′), 8.47 (d, 2H, bipy-H3 and 3′), 9.1 (d, 2H, bipy-H6 and 6′).

^{13}C NMR (200 MHz, CD_3CN, apt): δ/ppm = 124.0, 128.5, 129.7, 131.4, 142.1, 154.1 (quaternary C), 156.8, 182.4 (quaternary C), 187.1 (quaternary C).

2.3. Electrochemistry

Electrochemical experiments were performed using a JAISSLE Potentiostat–Galvanostat IMP 88 PC. A one-compartment cell was used for cyclic voltammetry experiments with a Pt working electrode, a Pt counter electrode and a Ag/AgCl quasi reference electrode calibrated with ferrocene/ferrocenium (Fc/Fc^+) as an internal reference. The half-wave potential ($E_{1/2}$) for Fc/Fc^+ was measured at

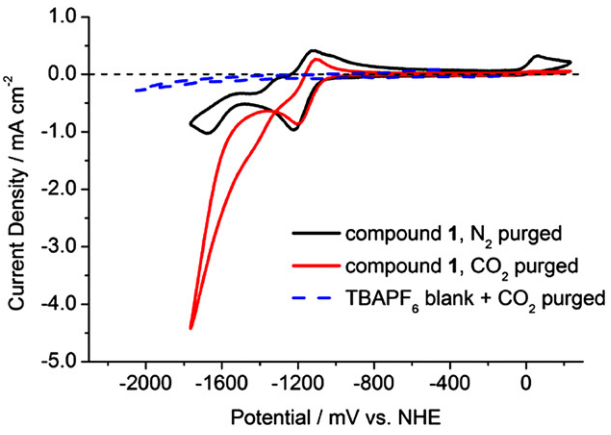

Fig. 1. Cyclic voltammograms of compound **1** in nitrogen- (black solid line) and CO_2-saturated electrolyte solution (red solid line), respectively. The scan in the presence of CO_2 shows large current enhancement due to a catalytic reduction of CO_2 to CO. Voltammograms are recorded at 100 mV s^{-1} in acetonitrile, Pt working electrode, Pt counter electrode, and a catalyst concentration of 1 mM. A scan with no catalyst present under CO_2 (blue dashed line) shows little to no reductive current. (For interpretation of the references to colour in this figure legend, the reader is referred to the web version of this article.)

407 mV vs. Ag/AgCl for the experiment shown in Fig. 1 and at 403 mV vs. Ag/AgCl for the experiment shown in Fig. 2. For the recalculation to NHE potential the $E_{1/2}$ for Fc/Fc^+ vs. NHE was taken at 640 mV as suggested by Bazan et al. [24].

All electrochemical experiments were performed in acetonitrile with 0.1 M tetrabutylammonium hexafluorophosphate ($TBAPF_6$) as supporting electrolyte. The solutions were purged with N_2 or CO_2 under stirring for 15 min before cyclic voltammograms were taken. The catalyst concentration in all cyclic voltammogram experiments was 1 mM, the CO_2 concentration was assumed to be at gas saturation of 0.28 M in acetonitrile [25]. Scheme 2 shows a schematic picture of the one-compartment cell for controlled potential electrolysis during CO_2 purging (A) and during electrolysis experiment (B).

2.3.1. Controlled potential electrolysis

Controlled potential electrolysis experiments were performed in a gas tight one-compartment and an H-cell with a Pt working electrode, a Pt counter electrode and a Ag/AgCl quasi reference electrode using ferrocene (Fc/Fc^+) as an internal reference. The one-compartment cell contained 14 ml of electrolyte solution and 10 ml gas phase. The H-cell contained 44 ml of electrolyte solution and 26 ml of gas phase in total. The two compartments of the H-cell were separated by a glass drip. Controlled potential electrolysis experiments were performed with and without stirring (compare Table 2).

2.4. GC- and FTIR measurements

FTIR measurements were performed on a BRUKER IFS 66/S FTIR spectrometer with 4 cm^{-1} spectral resolution. GC analysis was conducted on a Fisons GC 8000 with hot wire detector (HWD), 45/60 Carboxen 1000 column and helium as carrier gas at a flow rate of 30 ml min^{-1} and a temperature of 225 °C.

For Faradaic efficiency calculations, gas samples were taken from single-compartment cells and H-cells and the results are summarized in Table 2. For the FTIR measurements, a gas tight transmission cell (see Scheme 3) with ZnSe windows was designed to measure IR absorption in transmission mode. The spectra were recorded with and without 5 ml headspace sample after 10 min, 25 min and 50 min electrolysis experiments of compound **2** in

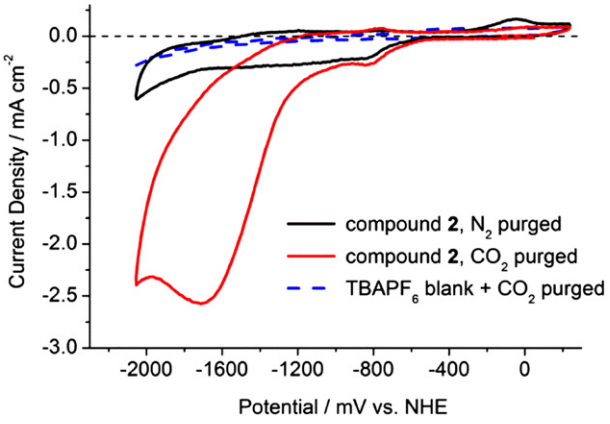

Fig. 2. Cyclic voltammograms of compound **2** in nitrogen- (black solid line) and CO_2-saturated electrolyte solution (red solid line), respectively. The scan in the presence of CO_2 shows a large current enhancement due to a catalytic reduction of CO_2 to CO. Voltammograms are recorded at 100 mV s^{-1} in acetonitrile, Pt working electrode, Pt counter electrode, and a catalyst concentration of 1 mM. A scan with no catalyst present under CO_2 (blue dashed line) shows little to no reductive current. (For interpretation of the references to colour in this figure legend, the reader is referred to the web version of this article.)

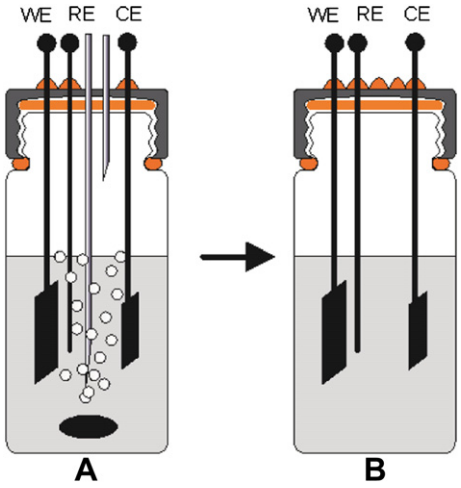

Scheme 2. One-compartment cell for controlled potential electrolysis during CO_2 purging (A) and during closed electrolysis experiment (B). Cells containing working electrode (WE), reference electrode (RE) and counter electrode (CE).

solution. For calibration of the systems, a defined amount of calibration gas (Linde) containing 11% CO_2, 1.5% CO, 600 ppm C_3H_8 and N_2 was used.

2.5. Photocatalytic reaction

Photocatalytic reactions were performed in a 10 ml quartz cell filled with 6 ml of a mixture of dimethylformamide and triethanolamine (DMF:TEOA = 5:1/v:v) containing a catalyst concentration of 2.6 mM under CO_2 saturation. The solution was stirred during the experiment and a 360 nm low pass cutoff filter was used. The irradiation time was 18 h under 26900 lux with an Osram 400 W Xenophot xenon lamp. The irradiated cell cross section area was 3.14 cm^2. Gas samples were taken with a syringe and transferred to FTIR gas analysis (for a schematic drawing see Scheme 3).

3. Results and discussion

3.1. Electrochemical studies

Fig. 1 shows the cyclic voltammograms of compound **1** measured in N_2 and CO_2 saturated acetonitrile solution, respectively.

Under N_2-saturated conditions, compound **1** showed similar features as already reported by Lehn et al. [19], namely a one-electron quasi-reversible reduction wave with its onset around −1080 mV vs. NHE followed by a one-electron irreversible reduction wave at more negative potential around −1530 mV vs. NHE.

Fig. 2 shows the cyclic voltammograms of compound **2** recorded under N_2- and CO_2-saturated conditions in acetonitrile solution.

In comparison to compound **1**, compound **2** doesn't show a clear separation between different reductive waves. Additionally the onset of the reductive current occurred at around −750 mV (vs. NHE) which is about 330 mV at more positive potential compared to compound **1** (Fig. 2).

When the acetonitrile solution was saturated with CO_2 both compounds showed a strong enhancement in the second reduction wave current density. Compound **1** shows a 4.5-fold increase in current density at the second irreversible reduction wave under CO_2 at −1750 mV (vs. NHE). The first quasi-reversible reduction wave does not show a significant increase in current density, (see Fig. 1). The compound **2** shows a 6.5-fold increase in current

Table 2
Summary of electrolysis experiments and efficiency calculations for CO_2 reduction to CO mediated by 1 mM concentration of compound **1** and compound **2**, respectively, in CO_2 saturated acetonitrile solution with 0.1 M $TBAPF_6$ at a constant potential of −1950 mV (vs. NHE) unless otherwise stated.

System	Stirring	Time/min	Method	Efficiency/%
1[a]	No	10	GC	50
2[a]	No	25	GC	43
2[a]	No	25	FTIR	45
2[a]	Yes	25	FTIR	24
2[a]	Yes	50	FTIR	27
2[b]	Yes	50	FTIR	28
1[b,c]	Yes	35	FTIR	31

[a] Experiments performed in a single-compartment cell.
[b] Experiments performed in a H-cell.
[c] At −1750 mV (vs. NHE).

density at the second irreversible reduction wave under CO_2 at −1750 mV (vs. NHE; Fig. 2). Although the relative increase in current density is higher for compound **2**, the absolute value for the current density of compound **1** (−3.47 mA cm^{-2}) is about 1.4 times higher than for compound **2** with about (−2.56 mA cm^{-2}) at −1750 mV (vs. NHE).

Fig. 3 shows the comparison of the first and second reduction for compounds **1** and **2** under a CO_2 atmosphere.

Fig. 1 shows a crossing of cathodic and anodic currents at around −1.3 V under CO_2. This trace crossing observed for compound **1** indicates the occurrence of a chain process where a species, which is easier reduced than the initial compound, is continuously produced and reduced at the electrode until the trace crossing disappears. This phenomenon has been previously observed and quantitatively interpreted for cyclic voltammetry measurements of electrocatalytic reduction processes [26–28].

One possible explanation is the formation of a dimer species in lack of sufficient CO_2 present which then can be further reduced to a dimer-anion [29–31]. These predictions agree with the experimental observations that trace crossing is enhanced with increasing catalyst concentration and with lower scan rates (compare Supplementary S1 and S2).

The catalytic rate constant (k) can be estimated from the cyclic voltammetry experiments. For a reversible electron-transfer process followed by a fast catalytic reaction the catalytic current (i_c) is given by equation (1) [32].

$$i_c = nFA[\mathrm{cat}]\sqrt{Dk[Q]^y} \quad (1)$$

Where n is the number of electrons involved in the catalyst reduction, F is the Faraday constant, A is the electrode area, [cat] is the catalyst concentration, D is the diffusion coefficient of the active catalytic species, [Q] is the concentration of the substrate (in this case CO_2) and y is the order of the substrate in the reaction in question.

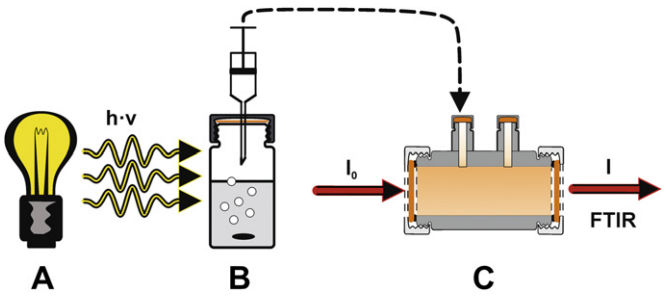

Scheme 3. Illustration of the photochemical CO_2 reduction experiment with the light source (A), the gas tight reaction cell (B) and the FTIR measurement cell (C).

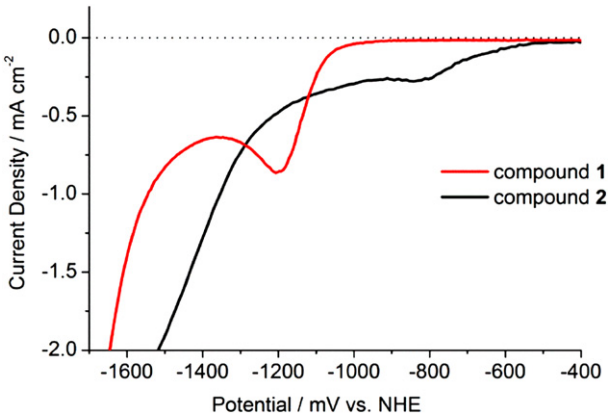

Fig. 3. Reductive current of compound **1** (red solid line) compared to compound **2** (black solid line) under CO_2 in saturated electrolyte solution. The second reduction wave of compound **2** occurs at ca. 300 mV more positive potential compared to compound **1**. Voltammograms are recorded at 100 mV s^{-1} in acetonitrile, Pt working electrode, Pt counter electrode, and a catalyst concentration of 1 mM. (For interpretation of the references to colour in this figure legend, the reader is referred to the web version of this article.)

Equation (2) can be used to determine the peak current (i_p) of a compound with a reversible electron transfer and no following reaction [33].

$$i_p = 0.446n^{3/2}FA[\mathrm{cat}]\sqrt{\frac{DF\nu}{RT}} \quad (2)$$

Where ν is the applied scan rate. The ratio of i_c to i_p measured in the cyclic voltammetry experiments shown in Figs. 1 and 2 can then be used to estimate k according to equation (3) [34,35].

$$\frac{i_c}{i_p} = \frac{1}{0.446}\sqrt{\frac{RT}{nF}}\sqrt{\frac{k[Q]^y}{\nu}} \quad (3)$$

Using the value of 2.1 for the ratio of i_c to i_p measured for compound **1** in equation (3) yields in a rate constant of about 60 M^{-1} s^{-1} which is in good agreement to literature values [36]. Applying the same method to our new compound **2** gives a ratio of i_c to i_p of 8.0 and hence a higher rate constant of about 220 M^{-1} s^{-1}.

3.2. GC and FTIR measurements

For a direct proof of the catalytic CO_2 reduction capability of compounds **1** and **2**, headspace gas samples were taken and analysed regarding the CO concentration by using FTIR and GC. For the FTIR absorption measurements a special gas tight IR transparent measurement cell containing two ZnSe windows was developed in our laboratory (for a schematic drawing see Scheme 3). This method has, compared to standard GC analysis, several advantages. The IR measurement has a very short measurement time, high reproducibility, works at ambient temperatures and pressures, shows no vulnerability to interact with a mobile or stationary phase and the gas sample will not come in contact with the detector system.

Fig. 4 shows a typical IR difference absorption spectrum in transmission mode. The two peaks centred around 2143 cm^{-1} correspond to the infrared active rotational–vibrations of the P and R branch of gaseous CO. For further details see reference [37]. The absorption increase at 2350 cm^{-1} and the two double peaks centred around 3650 cm^{-1} correspond to the infrared active vibrations of CO_2.

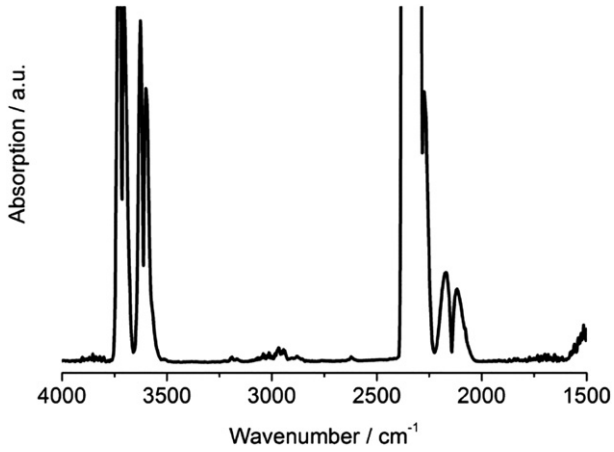

Fig. 4. IR difference absorption spectrum in transmission mode, with and without 5 ml headspace sample after 50 min electrolysis experiment of compound **2** in solution.

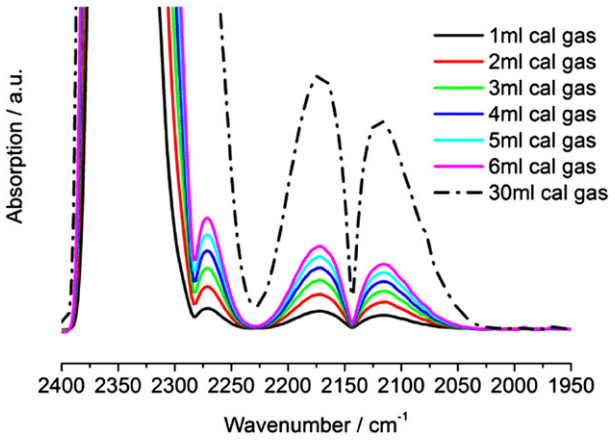

Fig. 5. IR difference absorption spectra in transmission mode, with different volumes of a N_2 calibration gas mixture containing 11% CO_2, 1.5% CO and 600 ppm C_3H_8. (The two peaks centred around 2143 cm^{-1} correspond to the infrared active vibration of CO, the peak at 2350 cm^{-1} to the vibrations of CO_2.)

The area under the peak can be determined by integration. Fig. 5 shows the calibration of the system by difference absorption spectra in transmission mode, with different volumes of a N_2 calibration gas mixture containing 11% CO_2, 1.5% CO and 600 ppm C_3H_8.

It was found that the peak area is linearly depending on the concentration of CO in the system (see Fig. 6).

With this setup, it was possible to determine the CO gas concentration in an initially N_2-filled transmission cell as low as 500 ppm.

Additionally, GC analysis was performed to confirm the results obtained from the FTIR measurements. Fig. 7 shows a typical gas chromatogram of a headspace sample from a 25 min CO_2 electrolysis experiment with compound **2** at a constant potential of −1950 mV (vs. NHE). The first peak corresponds to O_2 and N_2, which could not be separated with our system, the second to CO and the third to CO_2.

The results of both methods used for the quantitative investigation, FTIR absorption technique and GC analysis, are in good agreement (Table 2).

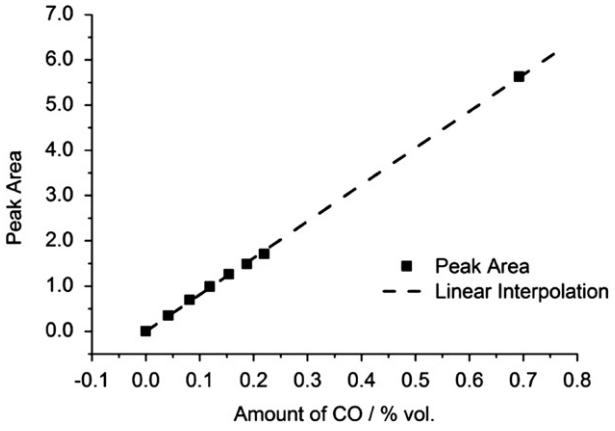

Fig. 6. Peak area of IR difference absorption peaks centred around 2143 cm^{-1} in transmission mode at different CO volumes (black squares) and linear interpolation between peak areas (black dotted line) from a reference gas calibration (11% CO_2, 1.5% CO and 600 ppm C_3H_8 in N_2).

3.3. Controlled potential electrolysis

Additional catalytic experiments have been performed to compare compound **1** as a benchmark compound with the new compound **2**. Controlled potential electrolysis at −1950 mV (vs. NHE) of both complexes was performed in acetonitrile solution saturated with CO_2 in a sealed cell. Experiments were either carried out in a one-compartment cell (for a schematic drawing see Scheme 2) or a H-cell with gas separated anode and cathode compartments. Headspace samples were taken and analysed regarding CO concentration with GC-analysis and FTIR absorption technique. For both compounds the Faradaic efficiency was determined according to equation (4).

$$\eta_{\text{Faradaic}} = \frac{\text{CO molecules in the gas phase} + \text{CO molecules in solution}}{2 \times \text{number of electrons put into the system}} \quad (4)$$

The number of moles CO in the gas phase was obtained by GC and FTIR analysis while the number of moles CO dissolved in the electrolyte solution was estimated by using Henrys Law with a Henry constant k_H of 2507 atm mol solvent per mol CO derived from data of Castillo et al. [38].

The results, summarized in Table 2, indicate that the compounds **1** and **2** performed comparable in terms of Faradaic efficiency. When the electrolyte solution was stirred during the controlled potential electrolysis, the Faradaic efficiency of both compounds dropped significantly in both the single-compartment and the H-cell setup. The independent values obtained from GC and FTIR data are in good agreement.

3.4. Electronic absorption spectra

Absorption features of the tricarbonylchlororhenium(I) polypyridyl complexes of the (LL)Re(CO)$_3$Cl-type are known to be sensitive to the nature of the solvent [18,22]. In Fig. 8 the absorption spectra of a dilute solution of compound **1** and compound **2**, respectively, in CO_2 saturated electrolyte solution are depicted.

In acetonitrile, compound **2** is characterized by a broad absorption maximum at around 375 nm and additional weaker UV-

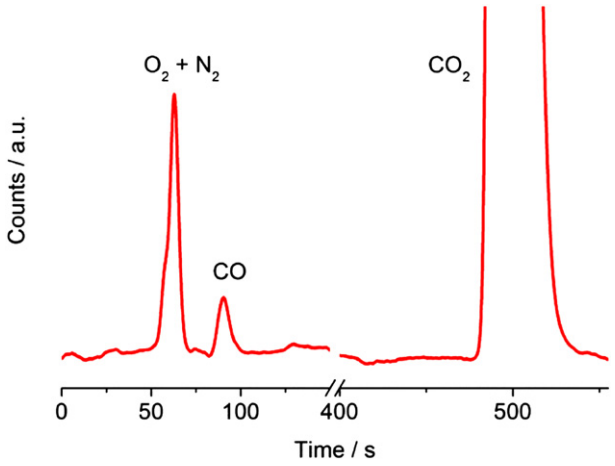

Fig. 7. GC analysis of a headspace sample (200 μl) after a 25 min electrolysis experiment with compound **2** in a single-compartment cell containing CO_2 saturated acetonitrile solution with $TBAPF_6$ (0.1 M), Pt working electrode, Pt counter electrode, and a catalyst concentration of 1 mM.

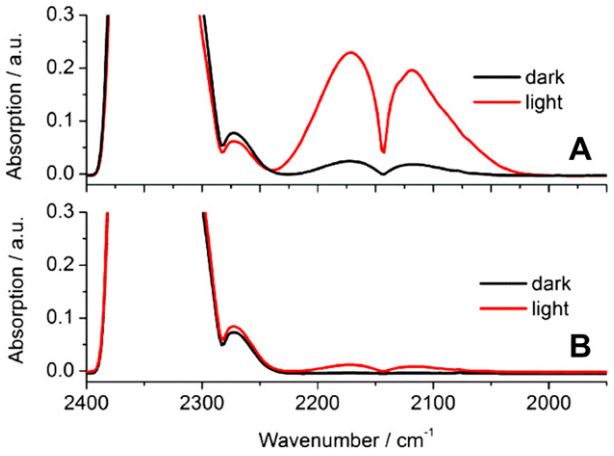

Fig. 9. IR difference absorption spectra (transmission mode) of headspace samples after illumination (red solid line) of a DMF:TEOA (5:1/v:v) solution with 2.6 mM catalyst concentration. Control dark experiments are also shown (black solid line). A, compound **1** and B, compound **2**. Light intensity 26900 lux, 360 nm low pass cutoff filter, irradiation time 18 h. (For interpretation of the references to colour in this figure legend, the reader is referred to the web version of this article.)

bands of intraligand transition origin occurring between 280 nm and 320 nm. Taking into account the typical negative solvatochromism of such metal complexes, these measurements are in good agreement with the previous results published by K. Oppelt et al. [22].

Fig. 8 shows a comparison of the UV–Vis absorption spectra of compounds **1** and **2**. Compound **2** shows a significantly increased absorption at the onset of the visible spectral region around 400 nm.

3.5. Photocatalytic CO_2 reduction

Fig. 9 shows FTIR gas analysis of a photocatalytic reduction experiment of a DMF/TEOA(5:1/v:v) solution containing 2.6 mM of compound **1** or **2**, respectively. The results were compared to a control experiment of the same solution kept in the dark. Headspace samples (5 ml) were taken after an irradiation time of 18 h and analysed by FTIR spectroscopy (for a schematic drawing see Scheme 3).

The spectra, as can be seen in Fig. 9, correspond to a CO gas concentration of A 22.38 vol% and B 0.98 vol% in 5 ml sample gas. As

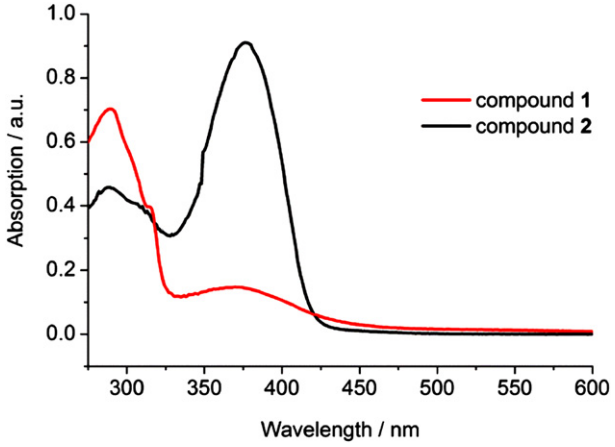

Fig. 8. Electronic absorption spectra of 6.25×10^{-5} M solutions of compound **1** and **2** in acetonitrile (298 K, 1-cm cell).

has been reported by other groups before, compound **1** showed high photocatalytic activity with a quantum yield of 8.7% [19,39]. In our experiment the new catalyst **2** showed a 22.8 fold lesser generation of CO under the same conditions as **1**. Taking this into account, our best estimate for the quantum yield of catalyst **2** (above 360 nm irradiation) is in the order of 0.4%.

4. Conclusion

In the present study, a new tricarbonylchlororhenium(I) polypyridyl complex (**2**) was investigated regarding to its potential as catalyst for homogeneous electrochemical and photochemical reduction of CO_2 to CO. The CO_2 reduction potential, determined by cyclic voltammetry occurs at ca. 300 mV more positive potential compared to compound **1**. The electrocatalytic activity of the new compound **2** is in the range of 45% for Faradaic efficiency for CO formation and ranks equally with the benchmark molecule **1**.

Additionally the new catalyst shows significantly higher absorption in the visible range, which was assumed to be a clear benefit for photocatalytic applications. However, the experiments over several hours of irradiation yielded only very low CO formation and under identical conditions, the unmodified compound **1** still performs better for photocatalytic CO_2 reduction. We attribute this different behaviour to an inversion of the lowest-lying excited state properties of compound **2** compared to the situation in compound **1**, which is crucial for the photochemical reactivity of such systems. Such an inversion from the typical metal-to-ligand charge transfer (MLCT) character present in **1** to an intraligand (IL) situation was already indicated in a more detailed photophysical study of the excited state deactivation pathways of complex **2** [22]. Further efforts should therefore focus on a systematic tuning of the excited state manifold of compounds such as **2** in order to better control the photocatalytic performance while at the same time improving the long-wavelength sensitization of the CO_2 reduction process [40].

Appendix A. Supplementary data

Supplementary data related to this article can be found online at http://dx.doi.org/10.1016/j.jorganchem.2012.05.021.

References

[1] R.A. Kerr, Science 317 (2007) 437.
[2] K. Richardson, W. Steffen, H.J. Schellnhuber, J. Alcamo, T. Barker, D.M. Kammen, R. Leemans, D. Liverman, M. Munasinghe, B. Osman-Elsha, N. Stern, O. Waever, Synthesis Report from Climate Change: Global Risks, Challenges & Decisions, University of Copenhagen, 2009.
[3] B. Kumar, J.M. Smieja, C.P. Kubiak, J. Phys. Chem. C 114 (2010) 14220–14223.
[4] A.J. Morrist, G.J. Meyer, E. Fujita, Acc. Chem. Res. 42 (2009) 1983–1994.
[5] M.D. Doherty, D.C. Grills, J.T. Muckerman, D.E. Polyansky, E. Fujita, Coord. Chem. Rev. 254 (2010) 2472–2482.
[6] M. Aresta, Carbon Dioxide as Chemical Feedstock, Wiley-VCH, Weinheim, 2010.
[7] H.A. Schwarz, R.W. Dodson, J. Phys. Chem. 93 (1989) 409–414.
[8] C.H. Hamann, A. Hamnett, W. Vielstich, Electrochemistry, WILEY-VCH, Weinheim, 1998, p. 372.
[9] S. Cosnier, A. Deronzier, J.C. Moutet, J. Electroanal. Chem. 207 (1986) 315–321.
[10] B.P. Sullivan, Electrochemical and Electrocatalytic Reactions of Carbon Dioxide, Elsevier, Amsterdam, 1993, p. 14.
[11] H. Arakawa, M. Aresta, J.N. Armor, M. Barteau, E.J. Beckman, T. Bell, J.E. Bercaw, et al., Chem. Rev. 101 (2001) 953–996.
[12] V. Balzani, A. Credi, M. Venturi, ChemSusChem 1 (2008) 26–58.
[13] J.M. Saveant, Chem. Rev. 108 (2008) 2348–2378.
[14] T. Yui, Y. Tamaki, K. Sekizawa, O. Ishitani, Top. Curr. Chem. 303 (2011) 151–184.
[15] E.E. Benson, C.P. Kubiak, A.J. Sathrum, J.M. Smieja, Chem. Soc. Rev. 38 (2009) 89–99.
[16] S.C. Roy, O.K. Varghese, M. Paulose, C.A. Grimes, ACS Nano 4 (2010) 1259–1278.
[17] G.A. Olah, A. Goeppert, G.K.S. Prakash, Beyond Oil and Gas: The Methanol Economy, WILEY-VCH, Weinheim, 2006, p. 212.
[18] K.D. Ley, K.S. Schanze, Coord. Chem. Rev. 171 (1998) 287–307.
[19] J. Hawecker, J.M. Lehn, R. Ziessel, Helv. Chim. Acta 69 (1986) 1990–2012.
[20] H. Takeda, O. Ishitani, Coord. Chem. Rev. 254 (2010) 346–354.
[21] J. Hawecker, J.M. Lehn, R. Ziessel, J. Chem. Soc. Chem. Commun. 6 (1984) 328–330.
[22] K. Oppelt, D.A.M. Egbe, U. Monkowius, M. List, M. Zabel, N.S. Sariciftci, G. Knör, J. Organomet. Chem. 696 (2011) 2252–2258.
[23] L.A. Worl, R. Duesing, P.Y. Chen, L. Dellaciana, T.J. Meyer, Chem. Soc. Dalton Trans. (1991) 849–858.
[24] C.M. Cardona, W. Li, A.E. Kaifer, D. Stockdale, G.C. Bazan, Adv. Mater. 23 (2011) 2367–2371.
[25] E. Fujita, D.J. Szalda, C. Creutz, N. Sutin, J. Am. Chem. Soc. 110 (1988) 4870–4872.
[26] C. Amatore, J. Pinson, J.M. Saveant, A. Thiebault, J. Electroanal. Chem. 107 (1980) 59–74.
[27] T.F. Connors, J.V. Arena, J.F. Rusling, J. Phys. Chem. 92 (1988) 2810–2816.
[28] A. Houmam, E.M. Hamed, M. Emad, I.W.J. Still, J. Am. Chem. Soc. 125 (2003) 7258–7265.
[29] B.P. Sullivan, C.M. Bolinger, D. Conrad, W.J. Vining, T.J. Meyer, J. Chem. Soc. Chem. Commun. 20 (1985) 1414–1416.
[30] F.P.A. Johnson, M.W. George, F. Hartl, J.J. Frantisek, Organometallics 15 (1996) 3374–3387.
[31] P. Christensen, A. Hamnett, A.V.G. Muir, J.A. Timney, J. Chem. Soc. Dalton Trans. 9 (1992) 1455–1463.
[32] J.M. Saveant, E. Vianello, Electrochim. Acta 8 (1963) 905–923.
[33] A.J. Bard, L.R. Faulkner, Electrochemical Methods, John Wiley, New York, 1980, p. 218.
[34] D.L. DuBois, A. Miedaner, R.C. Haltiwanger, J. Am. Chem. Soc. 113 (1991) 8753–8764.
[35] A. Miedaner, C.J. Curtis, R.M. Barkley, D.L. DuBois, Inorg. Chem. 33 (1994) 5482–5490.
[36] J.M. Smieja, C.P. Kubiak, Inorg. Chem. 49 (2010) 9283–9289.
[37] D.C. Harris, M.D. Bertolucci, Symmetry and Spectroscopy: An Introduction to Vibrational and Electronic Spectroscopy, Dover Pub., New York, 1978, pp. 121–127.
[38] Z.K. Lopez-Castillo, S.N.V.K. Aki, M.A. Stadtherr, J.F. Brennecke, Ind. Eng. Chem. Res. 45 (2006) 5351–5360.
[39] K. Koike, H. Hori, M. Ishizka, J.R. Westwell, K. Takeuchi, T. Ibusuki, K. Enjouji, H. Konno, K. Sakamoto, O. Ishitani, Organometallics 16 (1997) 5724–5729.
[40] G. Knör, U. Monkowius, Adv. Inorg. Chem. 63 (2011) 235–289.